Geoscience Frontiers 14 (2023) 101514

Contents lists available at ScienceDirect

Geoscience Frontiers

journal homepage: www.elsevier.com/locate/gsf

Research Paper

Generating soil thickness maps by means of geomorphological-empirical approach and random forest algorithm in Wanzhou County, Three Gorges Reservoir

Ting Xiao [a,b], Samuele Segoni [c], Xin Liang [b,*], Kunlong Yin [b], Nicola Casagli [c]

[a] Key Laboratory of Metallogenic Prediction of Nonferrous Metals and Geological Environment Monitoring, Ministry of Education, School of Geosciences and Info-Physics, Central South University, Changsha 410083, China
[b] Faculty of Engineering, China University of Geosciences, Wuhan 430074, China
[c] Department of Earth Sciences, University of Florence, Florence 50121, Italy

ARTICLE INFO

Article history:
Received 2 June 2022
Revised 20 September 2022
Accepted 20 November 2022
Available online 24 November 2022
Handling Editor: Biswajeet Pradhan

Keywords:
Soil thickness
Soil thickness mapping
Geomorphologically indexed soil thickness
Random forest

ABSTRACT

Soil thickness, intended as depth to bedrock, is a key input parameter for many environmental models. Nevertheless, it is often difficult to obtain a reliable spatially exhaustive soil thickness map in wide-area applications, and existing prediction models have been extensively applied only to test sites with shallow soil depths. This study addresses this limitation by showing the results of an application to a section of Wanzhou County (Three Gorges Reservoir Area, China), where soil thickness varies from 0 to ~40 m. Two different approaches were used to derive soil thickness maps: a modified version of the geomorphologically indexed soil thickness (GIST) model, purposely customized to better account for the peculiar setting of the test site, and a regression performed with a machine learning algorithm, i.e., the random forest, combined with the geomorphological parameters of GIST (GIST-RF). Additionally, the errors of the two models were quantified, and validation with geophysical data was carried out. The results showed that the GIST model could not fully contend with the high spatial variability of soil thickness in the study area: the mean absolute error was 10.68 m with the root-mean-square error (RMSE) of 12.61 m, and the frequency distribution residuals showed a tendency toward underestimation. In contrast, GIST-RF returned a better performance with the mean absolute error of 3.52 m and RMSE of 4.56 m. The derived soil thickness map could be considered a critical fundamental input parameter for further analyses.

1. Introduction

Soil thickness, often referred to by geotechnical engineers and geomorphologists as depth from the ground surface to the bedrock or depth to a marked change in geotechnical and hydrological properties (Catani et al., 2010). It has significant importance in numerous researches about the geology and environment, such as hillslope hydrology (Freer et al., 2002), slope stability (Ho et al., 2012; Basharat et al., 2018; Zhang et al., 2022a), seismic site effects (Rayhani and Naggar, 2008), landscape evolution (Heimsath et al., 2001), soil moisture distribution (Wang et al., 2001; Pellenq et al., 2003), dispersion of heat fluxes (Gochis et al., 2010), soil protection (Gabet and Dunne, 2003), and landslide hazard (Segoni et al., 2012; Cascini et al., 2017; Wang et al., 2019; Liang et al., 2022). In terms of data acquisition, direct or indirect measurements (e.g., borehole drilling or geophysical investigation) can be conducted to measure soil thickness on a local scale. However, when working on large areas, like basin-scale or region-scale studies, these methods are usually not affordable for reasons of time and cost. Therefore, some efficient approaches are needed to extrapolate the discrete soil thickness measurements to predict spatially exhaustive soil thickness maps, which could be used as input data for more complex environmental models.

The most straightforward and widely used approach to obtain soil thickness maps is through the empirical correlation with a digital terrain model (DTM)-derived morphometric attribute, such as slope, curvature, or elevation (Derose, 1996; Saulnier et al., 1997; Salciarini et al., 2006; Blesius and Weirich, 2009). Some authors have proposed more complex correlation schemes, which link soil thickness to a series of environmental and morphometric

* Corresponding author at: Faculty of Engineering, China University of Geosciences, Lumo Road 388, Hongshan District, Wuhan 430074, Hubei, China.
E-mail address: lxliangxin@cug.edu.cn (X. Liang).

https://doi.org/10.1016/j.gsf.2022.101514
1674-9871/

parameters utilizing multivariate statistical models (Odeh et al., 1994; Tsai et al., 2001; Pelletier and Rasmussen, 2009; Tesfa et al., 2009; Basharat et al., 2018). Catani et al. (2010) passed from simple morphometric attributes to more complex geomorphological factors and used the latter to establish an empirical correlation with soil thickness. Later, Soldato et al. (2016, 2018) improved this model and applied it to an area with pyroclastic soil cover. In other cases, regression kriging (Kuriakose et al., 2009) or machine learning algorithms were employed to define the soil thickness maps at the basin scale (Lagomarsino et al., 2017) and even at the national scale (Lacoste et al., 2016). In addition, some researchers analyzed the spatial variability of soil thickness through process-based models, which directly consider the formation mechanisms of the soil (e.g., Heimsath et al., 1999, 2001; Saco et al., 2006). These methods are mainly used to reconstruct or predict soil thickness variations in the landscape evolution framework on a geological time scale, which are more challenging to apply for mapping purposes.

In recent literature, two major issues remain when considering these aforementioned models. First, most soil thickness prediction methods have been tested in areas with relatively homogeneous geological conditions, mainly to model shallow soils with a thickness contained within a few meters. As a consequence, the possibility of applying these techniques is limited to case studies with well-constrained physical characteristics. Second, many wide-area practices perform a partition of the area into soil thickness classes rather than providing spatially exhaustive maps of continuous soil thickness values, which may hamper its application to other hydrologic and ecological models. Moreover, applying machine learning algorithms in soil thickness modelling is still a new attempt that needs further exploration of its use strategies and predictive capability in complex geological environments.

The main objective of this paper is to report on a first attempt to overcome these limits and validate the applicability of the thickness models in a complex geological setting (e.g., an area with different geological units with contrasting physical characteristics) with soil thickness extending from zero to several decametres. From a methodological point of view, we also aim to examine the feasibility of using machine learning algorithms to enhance the prediction accuracy of soil thickness. For this purpose, a 27 km^2 section of the Three Gorge Reservoir area (China) was selected as a test site. Two state-of-the-art methods, namely the geomorphologically indexed soil thickness (GIST) model (Catani et al., 2010) and the random forest machine learning algorithm, were significatively modified to effectively face the challenging objective. The GIST model was customized to better take into account the peculiar characteristics of the study area, while the random forest was run including in the list of the input parameters the geomorphological indexes of GIST, thus obtaining a hybridized version of the two methods. The results were then validated, compared, and discussed from the perspective of using the obtained soil thickness maps as support for forthcoming applications of other environmental models.

2. Test site description

The study area is located between 108°27′49″E–108°30′57″E and 30°49′32″N–30°53′25″N in the Three Gorges Area (Chongqing Municipality, southwestern China). It is a 27 km^2 section of Wanzhou County, comprising about 10 km from Tangjiao Village to Dazhou Town. The Yangtze River flows across the study area from SW to NE, which is close to urban infrastructure and human activities (Fig. 1). This region belongs to the subtropical humid monsoon zone and features a mild climate with abundant sunshine (Xiao et al., 2019a; Liang et al., 2021). The area is a hilly landscape with an overall step-like morphology formed by multi-level fluvial terraces, resulting from repeated tectonic uplift stages and the Yangtze River erosion (Xiao et al., 2019b). The geology of the area is characterized by layers of purple-red mudstone and sandstone (Shaximiao Formation of the Middle Jurassic) and red–purple quartz sandstone with interbedded mudstone (Suining Formation of Upper Jurassic). The bedrock is typically covered by Quaternary loose material with a thickness of 0–40 m.

3. Materials and methods

The overall workflow related to soil thickness modelling is presented in Fig. 2. The process consists of four main steps. First is the preparation and pre-processing of the input data. Second is the customization of the GIST model for the study area with step-like topography. Three morphometric factors (*C*, *P* and *S*, which related to profile curvature, position along the hillslope profile, and slope gradient, respectively) and an empirical parameter (*K*, representing the maximum soil thickness) were determined in this process. The GIST soil thickness map was obtained by means of calibration functions. Afterwards, parameters *C*, *P* and *S* of the GIST model and the other three attributes (altitude, plan curvature, and terrain roughness index) were utilized as covariates of the GIST-RF model, and the random forest algorithm was adopted for soil thickness prediction. Finally, the proposed two soil thickness maps were analyzed and compared with filed data. The detail of the input data and modelling process is described as follow.

3.1. Input data

The data used in this study mainly include a DTM, a geological map, and soil thickness samples. The DTM was derived from a topographic map, with contour lines spacing of 2 m, provided by the Land and Resources Bureau of the Wanzhou District. The cell size of the raster DTM is 10 m × 10 m, which is a suitable resolution for the scale of this study.

Concerning soil thickness, it should be emphasized that the specific definition of soil can vary within each branch of environmental sciences. For instance, some studies may be interested only in the shallowest layers of material occupied and influenced by root apparatus (Masi et al., 2021); or in the volume of material interested by pedogenetic processes (Jones et al., 2012; Ma et al., 2019). In contrast, since the main objective of this research is to provide some data that could be used in future activities concerning landslide hazard modelling and geotechnical engineering works on the slopes, soil thickness is intended here as the depth to bedrock, identified as the first marked change in hydrologic and mechanical properties (Catani et al., 2010). This definition of "soil" includes all the "soft" material (including, e.g., eluvium, colluvium, organic matter or debris) that covers the underlying hard rocks. According to this interpretation, a total of 75 soil thickness direct measurements were carried out, all of which were from field drilling works (Moye, 1967). As shown in Fig. 3, the diamond bit of the drilling machine could penetrate the ground right to the bedrock while the cores could be lifted and placed in the barrels. Then, by observing the physical characteristics of the core, it was possible to recognize the interface between soil and bedrock and determine the soil thickness with great accuracy. Moreover, the sample points appear in Fig. 1 with the distribution of several lines because they were drilled on transects to better investigate the soil thickness distribution along with the hillslope profile.

3.2. Customization and application of the GIST model

The geomorphologically indexed soil thickness (GIST) model is an empirical approach combining morphometric attributes with

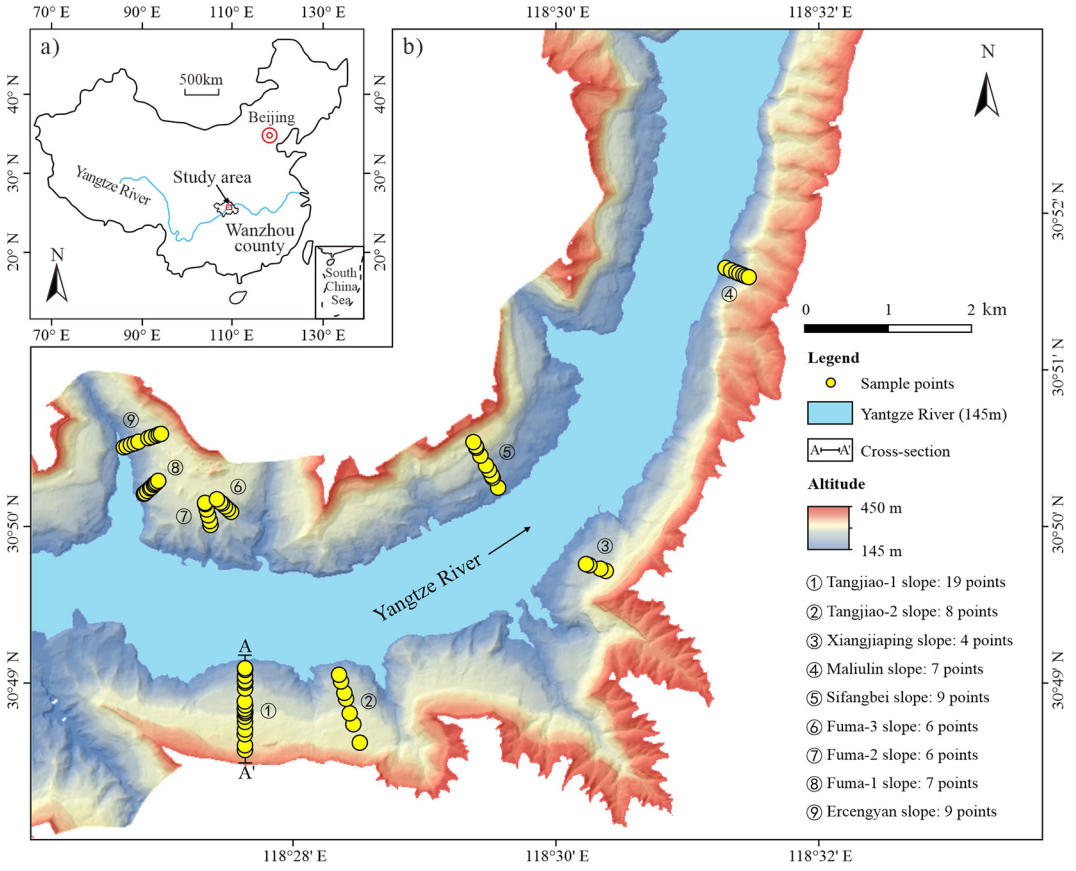

Fig. 1. Test site and location of the soil thickness measurements.

geomorphological and geological factors (Catani et al., 2010). This model includes three factors (*C*, *P*, and *S*) associated with morphometric attributes (curvature, position in the hillslope profile, and slope gradient, respectively) that influence soil thickness distribution. The factors, which will be described in detail below, can be easily derived from a DTM, have values ranging from 0 to 1 and are combined in the calibration function Eq. (1), where *K* is an empirical parameter representing the maximum possible soil thickness expected.

$$\text{Thickness} = K \times C \times P \times S \tag{1}$$

In this research, the value of *K* is set as the maximum thickness measured on the soil samples, while the three empirical factors *C*, *P* and *S* were assessed based on the procedure described in Catani et al. (2010), which was modified with site-specific customizations for the study area, as described in the following.

Factor *C* accounts for the effect of surface curvature. As reported by previous experiments and field observations, soil thickness in mature hillslopes is inversely correlated with the profile curvature of the slope since erosive creep-like processes prevail in convex morphologies, while concave morphologies are usually associated with accumulations of loose deposits at the footslope (Heimsath et al., 1999; Park et al., 2001). Following this theory, in the original version of the GIST model, factor *C* was calculated by rescaling the curvature values into values ranging from 0 to 1, according to a linear inverse correlation scheme. Similarly, in this study, the pixel-by-pixel profile curvature was derived from the DTM to get factor *C*. However, instead of adopting the straight inverse linear correlation scheme proposed by Catani et al. (2010), the curvature values were analyzed to consider a more refined correlation.

As shown in Fig. 4 although curvature values ranged from −120 to 91 in the study site, about 90.0% of curvature values were concentrated in the range from −4 to 4, with a mean value close to 0 and a standard deviation of 3.35. We interpreted the few values outside the −4 – 4 range as outliers, probably due to DTM imperfections, and we applied a linear inverse correlation with factor *C* only to profile curvature values inside this range. This procedure allowed a more thorough characterization of the representative values encountered at the test site. Anomalous convex and concave pixels were set to 0 and 1, respectively, highlighting the maximum possible propensity to erode or accumulate soil. The relationship linking profile curvature and factor *C* is translated into mathematical terms in Eq. (2), where *c* is the profile curvature.

$$C = \begin{cases} 0, & c > 4 \\ (4-c)/8, & -4 \leqslant c \leqslant 4 \\ 1, & c < -4 \end{cases} \tag{2}$$

Factor *P* accounts for the relative position within the hillslope profile. It is widely acknowledged that two points may exist with the same slope gradient and curvature but different soil thicknesses due to their own different position (Burt, 1986; Allison et al., 1993; Moore et al., 1993; Gessler et al., 1995). In order to illustrate the linkage between the relative position *p* of the point and its soil distribution within a hillslope profile, factor *P* was introduced into the GIST model (Catani et al., 2010; Tofani et al., 2017). As shown in Fig. 5 and Eq. (3), the index of position *p* can be determined by combining the shortest upslope distances α and downslope distances β based on the DTM in a geographic information system (GIS) (Tucker et al., 2001; Roering, 2008; Grieve et al., 2016):

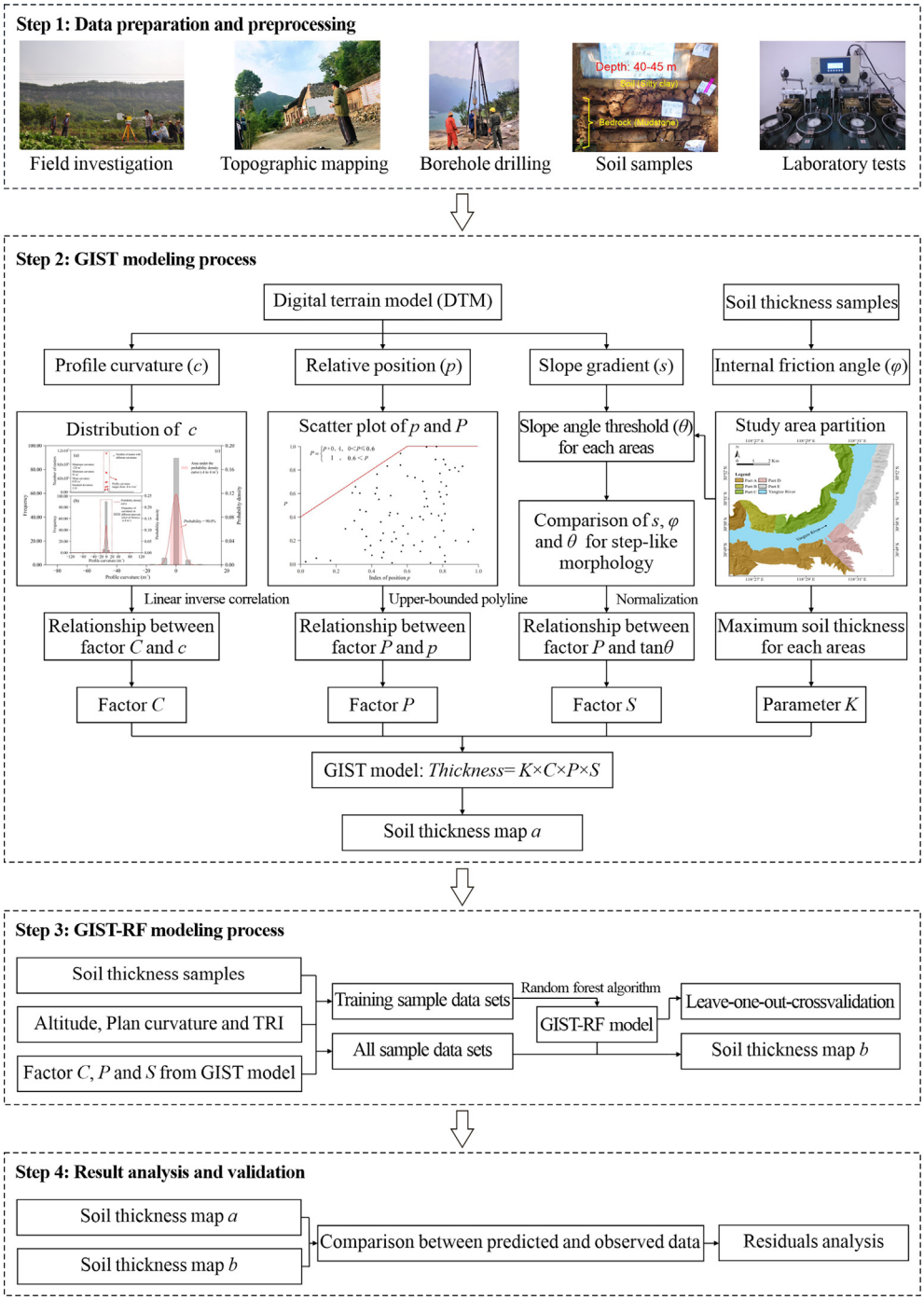

Fig. 2. Overall method used to generate soil thickness maps from GIST and GIST-RF model.

$$p = \alpha/(\alpha + \beta) \tag{3}$$

The relationship between p and soil thickness is highly site-specific and depends on the characteristics of the hillslope system (including bedrock features and geomorphic processes acting therein). Hence, to transform p into factor P, we did not rely on previously defined relationships (e.g., those used in Catani et al., 2010 or Tofani et al., 2017); rather, a new relationship was defined. In Fig. 6, for 75 control points, p was plotted versus the normalized thickness value, and it was verified that all points could be upper-bounded by a polyline; the equation of this polyline (Eq. (4)) was used to convert p into the factor P, which represents the normalized soil thickness expected in each position of the hillslope profile.

$$P = \begin{cases} p + 0.4, & 0 < p \leqslant 0.6 \\ 1, & 0.6 < p \end{cases} \tag{4}$$

The third factor of the GIST model, S, accounts for the effect of slope gradient, which plays a key role in mass wasting processes leading to soil loss (Roering et al., 2001; Montgomery and Brandon, 2002). Originally, Catani et al. (2010) coincived the factor S as a reduction factor acting only where local slope gradients overcome a specific slope threshold. Given the smooth landscape of their test site (a hilly basin in Chiantishire, Italy), factor S was not conceived to reflect the possibility that high slope gradients could be associated with the absence of soil (thickness equal to 0). As a consequence, in this study, the formulation of factor S is

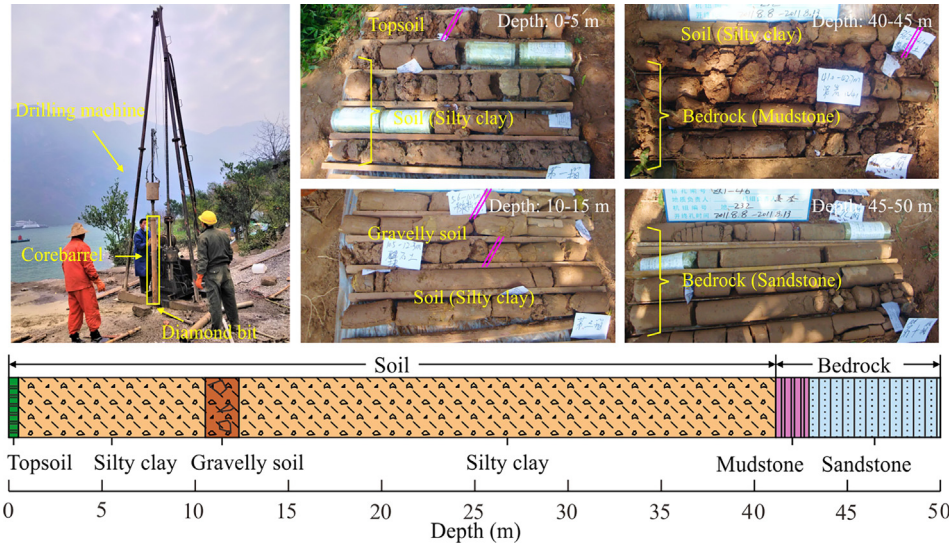

Fig. 3. Schematic diagram of the drilling investigation.

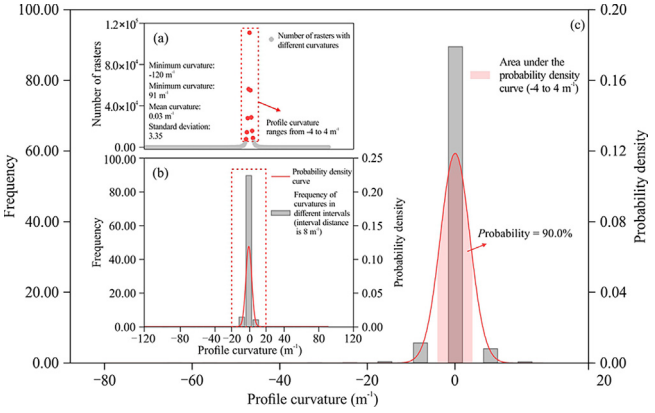

Fig. 4. Distribution of profile curvature in the study area.

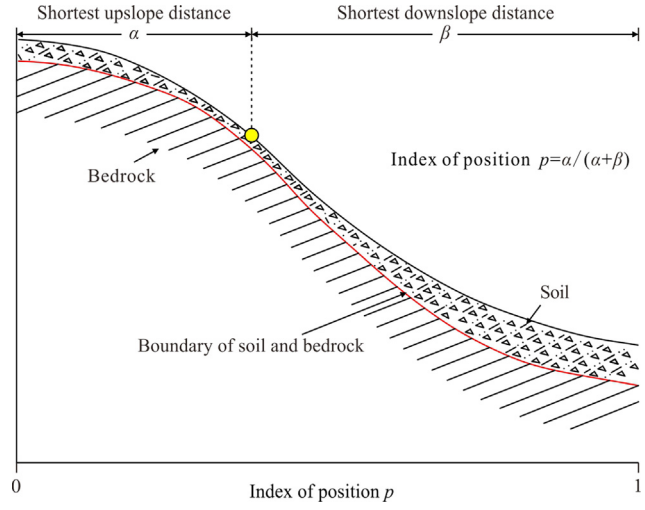

Fig. 5. A schematic representation of the index *p*, expressing the relative position of a point along the hillslope and calculated according to Eq. (3).

modified considering the step-like topography of the area. The value of factor *S* is assessed by a comparison between the slope

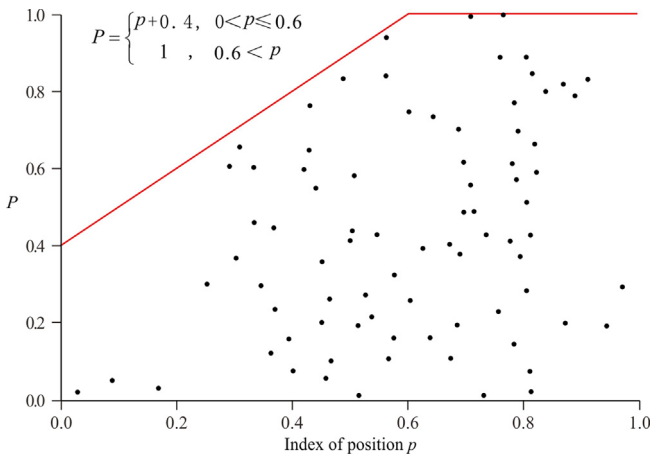

Fig. 6. Definition of the empirical relationship between the parameter *P* and the spatial position *p* in the study area.

gradient *s* (derived from the DTM) and two threshold angles: the internal friction angle of the soil φ and slope angle threshold θ. While the first is a mechanical property of soil that means the ability of soil to withstand shear stress and was measured by standardized laboratory tests (e.g., direct shear tests) on soil samples (Baker and Frydman, 2009), the latter was easily established by field investigations as it represents the slope gradient above which soil does not accumulate and the bare bedrock outcrops.

As shown in Eq. (5) when the value of the slope gradient is less than the internal friction angle, its effect on reducing soil thickness can be negligible. Under this circumstance, the value of the factor *S* is assigned as 1, leaving unaltered the maximum potential soil thickness expressed by the parameter *K* in Eq. (1). If the slope angle exceeds the threshold θ, the residual soil overlying the bedrock is assumed to be completely eroded or displaced by mass wasting processes, and the soil thickness is set as 0. When the slope gradient is between the threshold θ and φ, soil loss is considered proportional to the slope angle, as in Catani et al. (2010), to account for the effect of mass-wasting processes. According to the description above, local soil gradient *s* was derived pixel-by-pixel from the DTM, and factor *S* was computed using Eq. (5).

$$S = \begin{cases} 1, & 0 < s < \varphi \\ 1/(1+\tan\theta), & \varphi \leqslant s \leqslant \theta \\ 0, & \theta < s \end{cases} \quad (5)$$

To further customize the application of the GIST model to the test site, the values of φ and θ are not considered constant over the entire test area, as they depend on the soil and bedrock physical properties. Therefore, in order to get a better prediction result, the study area was divided into five partitions, supported by the differences observed in the typical φ values measured in the soil samples (Fig. 7 and Table 1).

Table 1
Model parameters in different parts of the study area. In each part, the value of φ was obtained by taking the mean value of the direct shear tests. The threshold θ was identified during the field investigation, corresponding to the minimum slope gradient associated with exposed bedrock where soil cannot accumulate. K is the calibration parameter of Eq. (1), and it is set as the maximum thickness measured on the soil samples in each part.

Parts	φ	θ	K (m)
A	14°	30°	40
B	17.15°	30°	31
C	19.83°	30°	34
D	9.43°	40°	23
E	17.38°	50°	36

3.3. GIST-RF model

The second soil thickness map of the study area was derived from a new prediction model named GIST-RF, which was created by hybridizing a random forest algorithm with the GIST model. The random forest algorithm is a nonparametric multivariate technique proposed by Breiman in 1995 and is considered a relatively robust approach in classification, regression, and unsupervised learning (Breiman 1996). It has since rapidly gained widespread consolidation through numerous research investigations and case studies (Pradhan et al., 2017; Zhang et al., 2019, 2021, 2022b; Segoni et al., 2020; Zhou et al., 2021). The random forest contains tree predictors that are generated using "bagging" to create multiple independent training sets. The random forest has excellent predictive performance and runs rapidly by summarizing a large number of classification trees; moreover, it is suitable for analyzing nonlinear variables without considering the matter of multicollinearity and is also robust for outliers in the predicted values. Compared to methods with single classifier combinations, the random forest has several advantages, including the simultaneous use of both categorical and numerical variables, prediction with "out-of-bag error" to avoid overfitting, and no requirement for a particular statistical distribution of the data (Breiman, 2001; Catani et al., 2013).

In geomorphological studies, random forest is usually applied using thematic or morphometric attributes (Zhang et al., 2022c). The main novelty of our approach is the combined use of morphometric attributes with the geomorphologically-based parameters of GIST. Along with the three parameters of GIST (C, S, and P), we included some attributes that are considered to be correlated with soil thickness (Saulnier et al., 1997; Salciarini et al., 2006; Blesius and Weirich, 2009), namely, altitude, plan curvature, and terrain roughness index (TRI). They were defined pixel-by-pixel through the GIS system and input into the GIST-RF model.

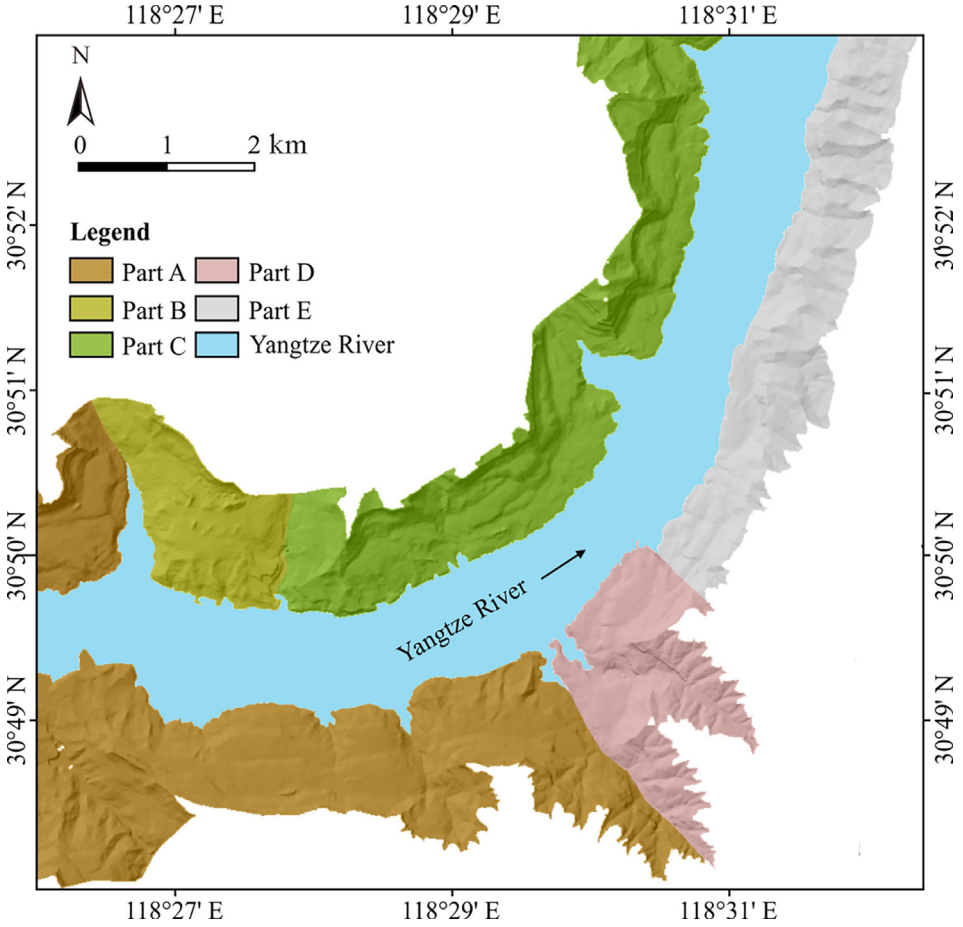

Fig. 7. Partition location map.

Random forest is a machine learning method that requires input data to train and iteratively optimize a prediction model. Most researchers prefer to select 70% of the sample data for training randomly, and the remaining 30% of the sample data is used to verify the reliability of the model (Segoni et al., 2020). However, there are only 75 observed points in our study area, which was not enough to be divided into two parts. Thus, the leave-one-out cross-validation was chosen to avoid the problem of insufficient training and verification data (Efron, 1982). In this method, 74 points were selected as training data for the random forest, and the remaining point was used for verification. This operation was repeated 75 times in the study until each point had a predicted value.

4. Results

The predictions of soil thickness exhibit highly different outputs through two models. As shown in Fig. 8a, the map produced by GIST model has the same thickness range from 0 to 40 m as the sample points. However, the soil depth generated by the GIST-RF model is more concentrated, ranging from 3.2 to 35.5 m and not covering the entire range of sampled values (Fig. 8b). Meanwhile, it can be easily seen that the spatial distribution of soil thickness values differs greatly. The left map (GIST model) portrays thinner soils with uneven values distribution, while on the right map, the depicted values have a marked spatial variability.

The prediction results using two models are compared to the measurements of 75 sample points for error quantification. A summary of accuracy is presented in Table 2, and a comparison between in-situ field data and the predictions is shown in Fig. 9. The 1:1 line, which could ideally represent perfect predictions, is employed to visualize the performance of the models. The values predicted using the GIST model have a poor correlation with the field data. On the contrary, the GIST-RF model exhibits good performance, with the square of the correlation coefficient accounting for 0.82 and root-mean-square error (RMSE) of 4.56 m. In terms of both mean error and mean absolute error, the estimation of soil thickness by the GIST model is substantial. The prediction values produced by the GIST model are systematically lower than field values, with an average error of about −9.81 m. This prediction trend is a consequence of the very shallow soils predicted in almost the entire study area (Fig. 8a). GIST-RF validation statistics are better than GIST: the mean error and average absolute errors made by GIST-RF are 0.04 m and 3.52 m, respectively. The absolute error of about 3.52 m may not be small in numerical terms, but if contextualized in this challenging case study, it represents an error lower than 9% of the range of the modelled values. This observation suggests that the GIST-RF model improves the performance of prediction data remarkably.

The performance of the models can be compared also on the basis of error frequency distribution. In the GIST model, the error is evenly distributed between −26.16 and 6.46 m (Fig. 10a), stressing the systematic underestimation of soil thickness in the study area again. The GIST-RF model returns a better result with smaller errors and exhibits a Gaussian distribution with a peak frequency of errors close to nearly zero (Fig. 10b).

5. Discussion

5.1. Validation of the GIST-RF model

To further test the reliability of the maps derived from the GIST-RF model, the modelled soil thickness was compared with a completely independent dataset obtained from the geophysical investigation. The multi-electrode resistivity method was employed in the Tangjiao Village to detect the geological structure below the ground surface. During the fieldwork, six transects were arranged in the test site with an electrode spacing of 5 m to detect the material resistivity (Fig. 11). As shown in Fig. 12, materials with different resistivity are marked in various colours. The red curve is the inferred boundary between the soil layer and bedrock. It is obvious that the soil distribution map predicted by the GIST-RF model is consistent with the trends of soil thickness measured using the geophysical method.

In addition, the longitudinal geological section of the Tangjiao-1 slope (A–A' in Fig. 1) is also selected to compare the predicted and observed results. The purple dotted line in Fig. 13 is the predicted interface from the soil map generated by the GIST-RF model (Fig. 8b), of which the ground elevation was taken from the DTM map, and subtraction of the predicted line thickness yields the bedrock. The solid red line in Fig. 13 shows the observed boundary of soil and bedrock drawn according to borehole drilling, exploratory trench, and field surveys. The horizontal length of the A–A' section

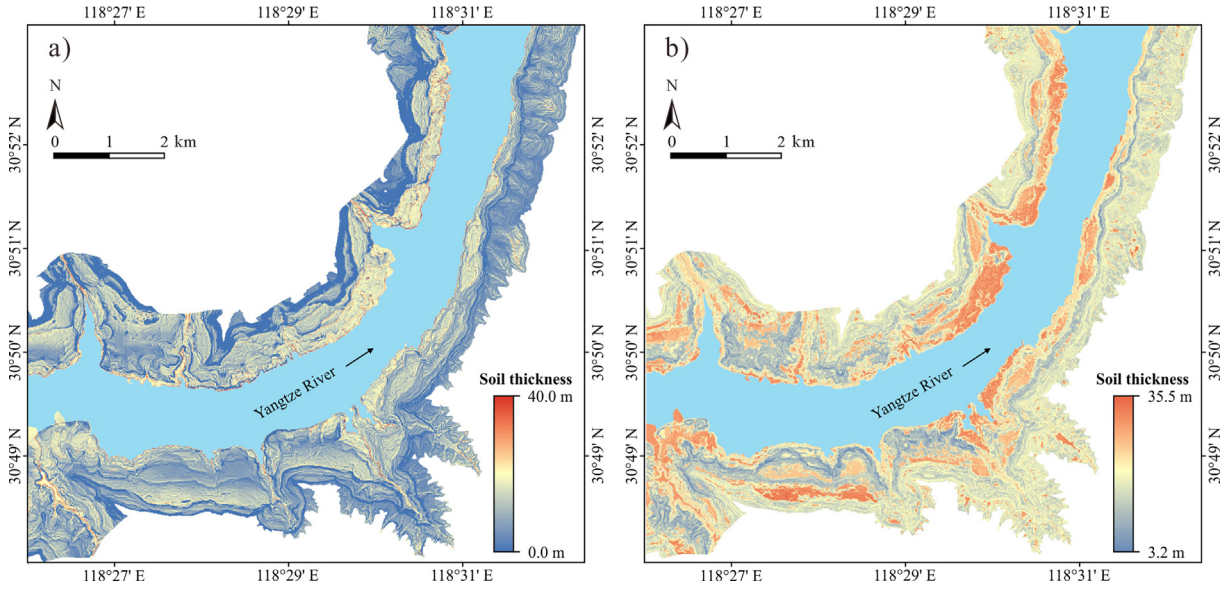

Fig. 8. Soil thickness map: (a) geomorphologically indexed soil thickness (GIST) model; (b) geomorphologically indexed soil thickness- random forest (GIST-RF) model.

Table 2
Comparison of validation results from geomorphologically indexed soil thickness (GIST) model and geomorphologically indexed soil thickness-random forest (GIST-RF) model.

Accuracy	Mean error (m)	Mean absolute error (m)	R-square	Root-mean-square error (RMSE) (m)
GIST model	−9.81	10.68	0.17	12.61
GIST-RF model	0.04	3.52	0.82	4.56

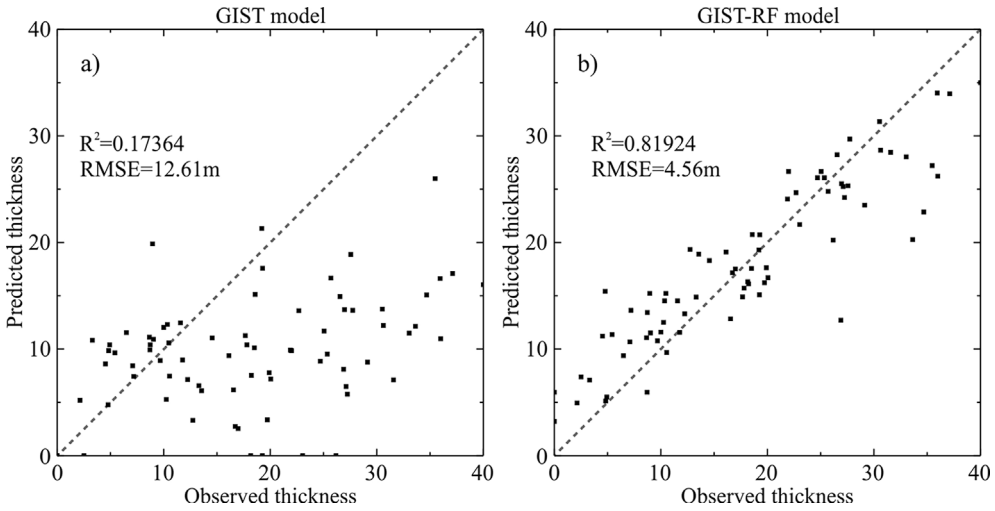

Fig. 9. Comparison between predicted and observed data.

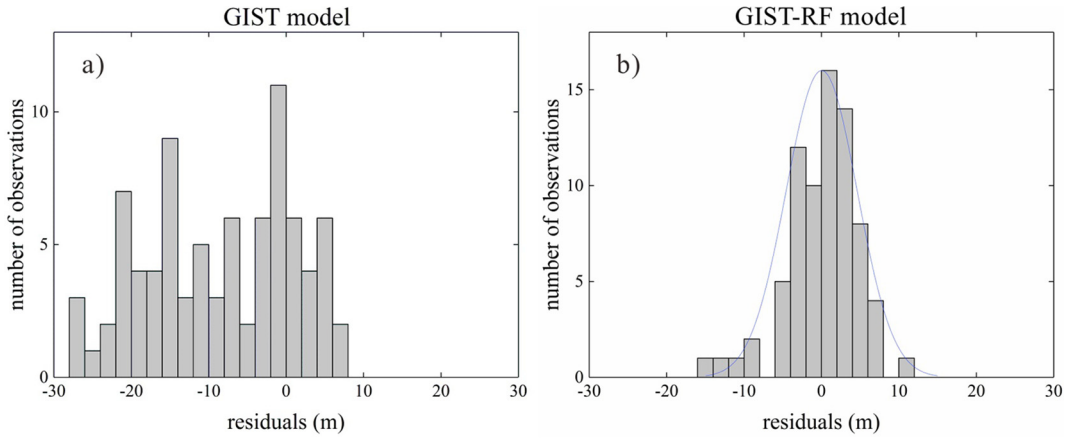

Fig. 10. Frequency distribution of residuals.

is about 1000 m, and the elevation ranges from 150 m to 370 m (Fig. 1). The elevation between 150 m and 175 m is in the hydro-fluctuation belt of the Three Gorges Reservoir. Specifically, the elevations of ~220 m, 260–280 m, and 300–320 m are the first, second, and third terrace platforms of the Yangtze River. According to the field investigation, the soil is mainly distributed at the platforms and the front edge of the slope, and the third terrace is slightly thicker than the other parts. In contrast, the soil is exposed to intense erosional processes in the steep ridges, so its depth is relatively small.

The general trend in the observed boundary is also produced in the interface predicted by the GIST-RF model. The soil thickness of some essential parts in Fig. 13, such as steep ridges and platforms, is similar to the observed profile, which means that the predicted results are reasonable. It should be mentioned that the slope gradient at the elevation of 320–370 m does not reach the threshold θ set in the model parameter, so the bedrock exposed here is modelled as a slope covered by a thin soil mantle. This phenomenon suggests that the slope angle threshold θ is critical to the model and must be selected after an extensive site-specific calibration.

5.2. Comparison of GIST model and GIST-RF model

As drawn by the result given in the last section, the GIST model returned an unsatisfactory result with errors evenly distributed between −26.1 m and 9.0 m, and the frequency distribution of residuals shows a marked tendency toward underestimation. Although the predicted soil thickness for the whole study area ranges from 0 m to 40 m, almost all values are smaller than 30 m. At the same time, a large area of the test site has a soil thickness of less than 10 m, which does not correspond to the real spatial distribution in the region. The GIST model is an empirical model, which was initially conceived to predict soil thickness to support distributed models for triggering shallow landslides, and the soil thickness modelled in such cases is within a few meters (Segoni et al., 2012; Mercogliano et al., 2013; Rossi et al., 2013).

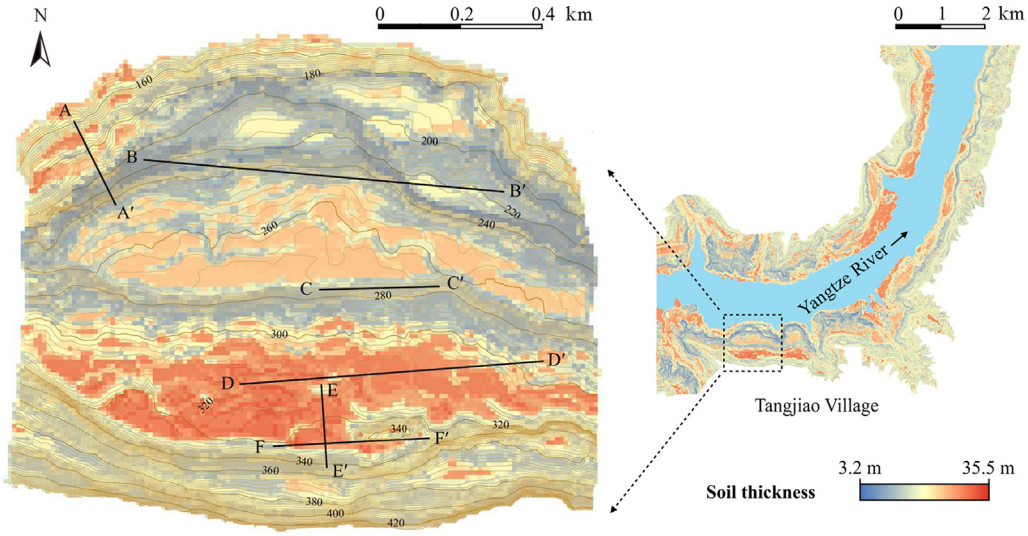

Fig. 11. The position of six transects in Tangjiao Village, where the underground resistivity was measured to infer soil thickness.

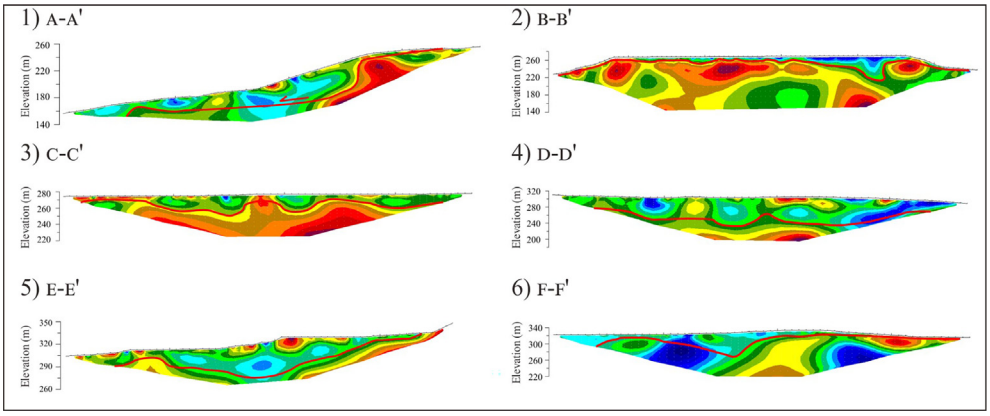

Fig. 12. Materials resistivity and inferred soil boundary from the geophysical investigation.

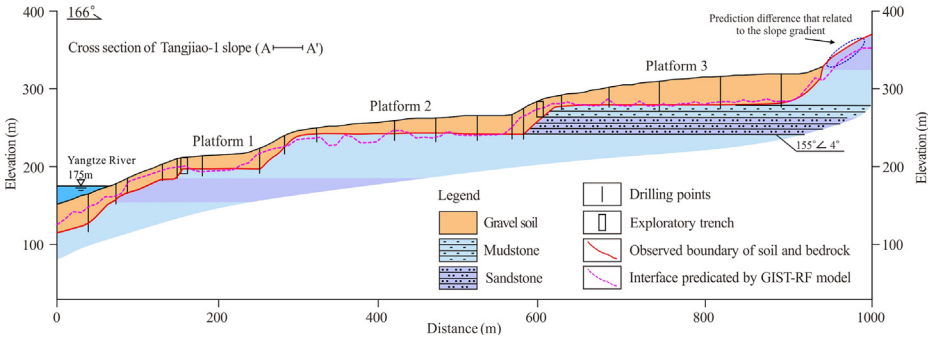

Fig. 13. Geological section of Tangjiao-1 slope.

In our case, however, the proposed application represents an attempt to stretch the limits of the GIST model through site-specific tuning and account for a larger interval of values in a different area. According to the field investigations, the soil thickness in the study area mainly varies between 10 m and 30 m, whereas near the scarps is almost less than 10 m. The Quaternary deposits at the leading edge and some local parts of the slope are characterized by a large thickness. From this point of view, the GIST model is not suitable for the thicker study area with a thick soil layer. The reason may be attributed to the complex genesis of the Three Gorges area, and the soil thickness cannot be obtained accurately using such a simple formula (Eq. (1)). A method based on empirical geomorphology must be highly site-specific; thus, it is understandable that the GIST model performed well in Italy (Catani et al.,

2010; Segoni et al., 2012) but exhibits less effectiveness in this section of Wanzhou County.

For the GIST-RF model, the importance of each variable is evaluated by means of the out-of-bag error (OOBE). For each variable, the importance was assessed based on the results of the leave-one-out cross-validation method. As a consequence, Fig. 14 shows the box plot of the variable importance distribution resulting from the 75 iterations of the random forest algorithm. The distribution of importance indicates that the parameters from the GIST model have a relatively high importance value, which provides a side view of the importance of the GIST model for soil thickness prediction.

According to the analysis of the mean error values between the two models, it is obvious that the performance of the GIST-RF model is more balanced, which is also confirmed by the statistical distribution of the scatter plot (Fig. 9) and the residual values (Fig. 10). This is important to avoid systematic overestimations or underestimations of soil thickness, which can propagate into other models that use soil thickness as an input parameter. Considering the large range of thickness values in our study area, the outcomes of the GIST-RF model (3.52 m average absolute error) are acceptable. In addition, the residual frequency exhibits a gaussian distribution with a peak frequency of errors nearly to zero, which indicates the outcomes of the GIST-RF model are reliable. As shown in Fig. 8, the range of predicted soil thickness values (from 3.2 to 35.5 m) in the whole region is smaller than the real range. It should be noticed that only two 0 m value points and only one 40 m value point were present among the 75 sample points. Due to the undersampling of the extreme values in the soil thickness range, the results of the GIST-RF model were more centred on the mean values. A statistical approach naturally tends to reflect the training dataset distribution. However, we think that the dataset used in the model calibration was representative of the study area, with carefully selected transects; therefore, the derived map should not be considered to be affected by significant systematic underestimations or overestimations induced by the dataset distribution. Compared to the GIST method, the GIST-RF model is more capable of accounting for interactions and nonlinearities between factors. In addition, the reliability of the GIST-RF model can be confirmed by the geophysical transects and the A–A' profile in Tangjiao Village.

GIST is a simple multiplication of geomorphological factors that the output thickness value is oversensitive to each factor. As long as one of the factors has a low value, the final output will be very small, which is the reason for the overall smaller predicted values of the GIST map (Fig. 8a). Therefore, for further developments on the GIST model: the empirical attributes it is based upon are valid, but the way they are combined together (the simple combination of Eq. (1)) seems to be the weak point of the procedure. GIST-RF combines the same (and similar) factors with the random forest algorithm, which is exactly a more sophisticated way to avoid heavy underestimations and get good results. Meanwhile, the random forest method is not the only choice to modify the GIST model; its application is an exploration of machine learning in soil thickness modelling. The further use of other types of machine learning methods would be a positive attempt to improve the prediction accuracy of soil thickness (Pradhan, 2013; Sameen et al., 2020).

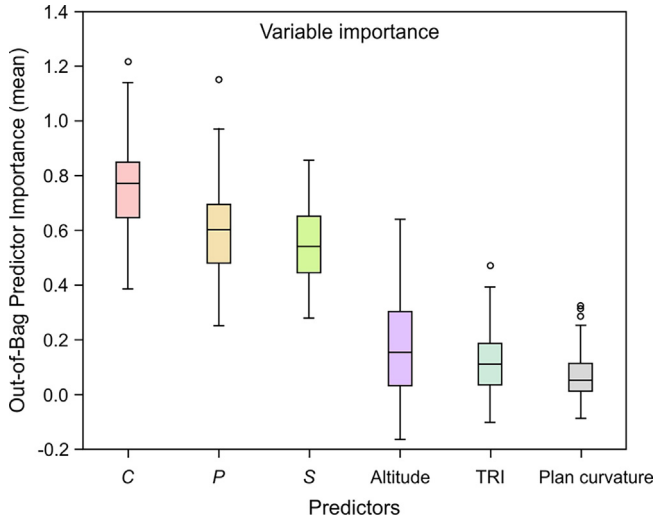

Fig. 14. Estimation of the relative importance of the predictors, including *C*, *P*, *S* from the GIST model and altitude, terrain roughness index (TRI), and plan curvature.

6. Conclusion

Two modified techniques are carried out to model spatially exhaustive soil thickness maps in a key section of Wanzhou County, China. This area features a wide range of soil thicknesses from 0 to ~ 40 m, which provides an opportunity to validate the applicability of state-of-the-art soil thickness prediction models in very challenging conditions. The geomorphologically indexed soil thickness (GIST) model is improved purposely to better fit the specific geology setting of the study area. In addition, a random forest based GIST-RF model, which used the geomorphological indexes of GIST, is also performed for comparison with the conventional GIST model.

The GIST-RF model yields better results than the GIST model. The mean absolute error of the predicted result utilized by the GIST-RF model is less than 9% of the whole range of the sampled value, and the peak frequency of errors is approximately close to 0 in a gaussian statistical distribution. Moreover, a well-aligned performance is also drawn from the qualitative comparison with geophysical resistivity transects and a specific profile. All the inspection of implementation results indicates that the GIST-RF model is considered superior and reliable.

This study demonstrates that a regression based on machine learning algorithms, with input parameters with geomorphological significance, can improve the predictions even in complex environmental settings characterized by complex geology and thick soil cover. In our case study, the application of random forest addresses the limitations of the GIST model and improves its performance, opening new perspectives to using other machine learning or deep learning algorithms to determine the spatial distribution of soil thickness.

Declaration of Competing Interest

The authors declare that they have no known competing financial interests or personal relationships that could have appeared to influence the work reported in this paper.

Acknowledgements

The authors acknowledge the following foundations for providing financial support for this work: National Natural Science Foundation of China (Grant Nos. 41877525, 61971037 and 31727901), and Chongqing Key Laboratory of Geological Environment Monitoring and Disaster Early-warning in Three Gorges Reservoir Area (No. MP2020B0301). The authors also thank the reviewers for their suggestions that improved the quality of this paper.

Data and codes availability statement

The relevant datasets in this study are available from the corresponding author on request.

References

Allison, R.J., Goudie, A.S., Cox, N.J., 1993. Geotechnical properties of rock masses: their control on slope form and mechanisms of change along the Napier Range, Western Australia. Geomorphology 8 (1), 65–80. https://doi.org/10.1016/0169-555X(93)90004-L.

Baker, R., Frydman, S., 2009. Unsaturated soil mechanics: critical review of physical foundations. Eng. Geol. 106 (1–2), 26–39. https://doi.org/10.1016/j.enggeo.2009.02.010.

Basharat, M., Qasim, M., Shafique, M., Hameed, N., Riaz, M.T., Khan, M.R., 2018. Regolith thickness modeling using a GIS approach for landslide distribution analysis, NW Himalayas. J. Mt. Sci. 15 (11), 2466–2479. https://doi.org/10.1007/s11629-018-4840-6.

Blesius, L., Weirich, F., 2009. The use of high-resolution satellite imagery for deriving geotechnical parameters applied to landslide susceptibility. In: Proceedings of the ISPRS Hannover Workshop 2009 on High-resolution Earth Imaging for Geospatial Information, Hannover, Germany, 2-5.

Breiman, L., 1996. Bagging predictors. Mach. Learn. 24 (2), 123–140. https://doi.org/10.1007/BF00058655.

Breiman, L., 2001. Random forests. Mach. Learn. 45 (1), 5–32. https://doi.org/10.1023/A:1010933404324.

Burt, T.P., 1986. Slopes and slope processes. Prog. Phys. Geogr. 10 (4), 547–562. https://doi.org/10.1177/030913339101500405.

Cascini, L., Ciurleo, M., Di, N.S., 2017. Soil depth reconstruction for the assessment of the susceptibility to shallow landslides in fine-grained slopes. Landslides 14 (2), 459–471. https://doi.org/10.1007/s10346-016-0720-8.

Catani, F., Segoni, S., Falorni, G., 2010. An empirical geomorphology-based approach to the spatial prediction of soil thickness at catchment scale. Water Resour. Res. 46 (5), 1–15. https://doi.org/10.1029/2008WR007450.

Catani, F., Lagomarsino, D., Segoni, S., Tofani, V., 2013. Landslide susceptibility estimation by random forests technique: sensitivity and scaling issues. Nat. Hazards Earth Syst. Sci. 13 (11), 2815–2831. https://doi.org/10.5194/nhess-13-2815-2013.

Derose, R.C., 1996. Relationships between slope morphology, regolith depth, and the incidence of shallow landslides in eastern Taranaki hill country. Z. Geomorphol. 105, 49–60.

Efron, B., 1982. The Jackknife, the Bootstrap and Other Resampling Plans. Society for Industrial and Applied Mathematics, Philadelphia, p. 100.

Freer, J., McDonnell, J.J., Beven, K.J., Peters, N.E., Burns, D.A., Hooper, R.P., Aulenbach, B., Kendall, C., 2002. The role of bedrock topography on subsurface storm flow. Water Resour. Res. 38 (12), 1–16. https://doi.org/10.1029/2001WR000872.

Gabet, E.J., Dunne, T., 2003. A stochastic sediment delivery model for a steep Mediterranean landscape. Water Resour. Res. 39 (9), 1237–1249. https://doi.org/10.1029/2003WR002341.

Gessler, P.E., Moore, I.D., Mckenzie, N.J., Ryan, P.J., 1995. Soil-landscape modelling and spatial prediction of soil attributes. Int. J. Geogr. Inf. Sci. 9 (4), 421–432. https://doi.org/10.1080/02693799508902047.

Gochis, D.J., Vivoni, E.R., Watts, C.J., 2010. The impact of soil depth on land surface energy and water fluxes in the North American monsoon region. J. Arid. Environ. 74, 564–571. https://doi.org/10.1016/j.jaridenv.2009.11.002.

Grieve, S.W., Mudd, S.M., Hurst, M.D., 2016. How long is a hillslope? Earth Surf. Process. Landf. 41 (8), 1039–1054. https://doi.org/10.1002/esp.3884.

Heimsath, A.M., Dietrich, W.E., Nishiizumi, K., 1999. Cosmogenic nuclides, topography, and the spatial variation of soil depth. Geomorphology 27, 151–172. https://doi.org/10.1016/S0169-555X(98)00095-6.

Heimsath, A.M., Chappell, J., Dietrich, W.E., Nishiizumi, D., Finkel, R.C., 2001. Late Quaternary evolution in southeastern Australia: a field example using cosmogenic nuclides. Quat. Int. 83, 169–185. https://doi.org/10.1016/S1040-6182(01)00038-6.

Ho, J.Y., Lee, K.T., Chang, T.C., Wang, Z.Y., Liao, Y.H., 2012. Influences of spatial distribution of soil thickness on shallow landslide prediction. Eng. Geol. 124, 38–46. https://doi.org/10.1016/j.enggeo.2011.09.013.

Jones, A., Panagos, P., Barcelo, S., Boraoui, F., Bosco, C., Dewitte, O., Gardi, C., Erhard, M., Hervás, J., Hiederer, R., 2012. The State of Soil in Europe. European Environment Agency, Copenhagen.

Kuriakose, S.L., Devkota, S., Rossiter, D.G., Jettena, V.G., 2009. Prediction of soil depth using environmental variables in an anthropogenic landscape, a case study in the Western Ghats of Kerala, India. Catena 79(1), 27-38. doi:10.1016/j.catena.2009.05.005.

Lacoste, M., Mulder, V.L., Richer-de-Forges, A.C., Martin, M.P., Arrouays, D., 2016. Evaluating large-extent spatial modeling approaches: a case study for soil depth for France. Geoderma Reg. 7 (2), 137–152. https://doi.org/10.1016/j.geodrs.2016.02.006.

Lagomarsino, D., Tofani, V., Segoni, S., Catani, F., Casagli, N., 2017. A tool for classification and regression using random forest methodology: applications to landslide susceptibility mapping and soil thickness modeling. Environ. Model. Assess. 22 (3), 201–214. https://doi.org/10.1007/s10666-016-9538-y.

Liang, X., Gui, L., Wang, W., Du, J., Ma, F., Yin, K.L., 2021. Characterizing the development pattern of a Colluvial landslide based on long-term monitoring in the Three Gorges Reservoir. Remote Sens. 13 (2), 224. https://doi.org/10.3390/rs13020224.

Liang, X., Segoni, S., Yin, K.L., Du, J., Chai, B., Tofani, V., Casagli, N., 2022. Characteristics of landslides and debris flows triggered by extreme rainfall in Daoshi Town during the 2019 Typhoon Lekima, Zhejiang Province, China. Landslides 19, 1735–1749. https://doi.org/10.1007/s10346-022-01889-5.

Ma, Y., Minasny, B., Malone, B.P., Mcbratney, A.B., 2019. Pedology and digital soil mapping (DSM). Eur. J. Soil Sci. 70 (2), 216–235. https://doi.org/10.1111/ejss.12790.

Masi, E., Segoni, S., Tofani, V., 2021. Root reinforcement in slope stability models: a review. Geosciences 11 (5), 212. https://doi.org/10.3390/geosciences11050212.

Mercogliano, P., Segoni, S., Rossi, G., Sikorsky, B., Tofani, V., Schiano, P., Catani, F., Casagli, N., 2013. Brief communication "A prototype forecasting chain for rainfall induced shallow landslides". Nat. Hazards Earth Syst. Sci. 13 (3), 771–777. https://doi.org/10.5194/nhess-13-771-2013.

Montgomery, D.R., Brandon, M.T., 2002. Topographic controls on erosion rates in tectonically active mountain ranges. Earth Planet. Sci. Lett. 201, 481–489. https://doi.org/10.1016/S0012-821X(02)00725-2.

Moore, I.D., Gessler, P.E., Nielsen, G.A., Peterson, G.A., 1993. Soil attribute prediction using terrain analysis. Soil Sci. Soc. Am. J. 57 (2), 443–452. https://doi.org/10.2136/sssaj1993.03615995005700020026x.

Moye, D.G., 1967. Diamond drilling for foundation exploration. Inst. Engrs. Civil Eng. Trans. 9 (1), 95–100.

Odeh, I.O.A., McBratney, A.B., Chittleborough, D.J., 1994. Spatial prediction of soil properties from a digital elevation model. Geoderma 63, 197–214.

Park, S.J., Mcsweeney, K., Lowery, B., 2001. Identification of the spatial distribution of soils using a process-based terrain characterization. Geoderma 103, 249–272. https://doi.org/10.1016/S0016-7061(01)00042-8.

Pellenq, J., Kalma, J., Boulet, G., Saulnier, G.M., Wooldridge, S., Kerr, Y., Chehbouni, A., 2003. A disaggregation scheme for soil moisture based on topography and soil depth. J. Hydrol. 276, 112–127. https://doi.org/10.1016/S0022-1694(03)00066-0.

Pelletier, J.D., Rasmussen, C., 2009. Geomorphically based predictive mapping of soil thickness in upland watersheds. Water Resour. Res. 45, (9). https://doi.org/10.1029/2008WR007319 w09417.

Pradhan, B., 2013. A comparative study on the predictive ability of the decision tree, support vector machine and neuro-fuzzy models in landslide susceptibility mapping using GIS. Comput. Geosci. 51, 350–365. https://doi.org/10.1016/j.cageo.2012.08.023.

Pradhan, B., Seeni, M.I., Nampak, H., 2017. Integration of LiDAR and QuickBird Data for Automatic Landslide Detection Using Object-Based Analysis and Random Forests. In: Pradhan, B. (Ed.), Laser Scanning Applications in Landslide Assessment. Springer, Cham, pp. 69–81. https://doi.org/10.1007/978-3-319-55342-9_4.

Rayhani, M.T., Naggar, M.H.E.I., 2008. Numerical modeling of seismic response of rigid foundation on soft soil. Int. J. Geomech. 8 (6), 336–346. https://doi.org/10.1061/(ASCE)1532-3641(2008)8:6(336).

Roering, J.J., 2008. How well can hillslope evolution models "explain" topography? Simulating soil transport and production with high-resolution topographic data. Geol. Soc. Am. Bull. 120, 1248–1262. https://doi.org/10.1130/B26283.1.

Roering, J.J., Kirchner, J.W., Sklar, L.S., Dietrich, W.E., 2001. Hillslope evolution by nonlinear creep and landsliding: an experimental study. Geology 29 (2), 143–146. https://doi.org/10.1130/0091-7613(2001)029<0143:HEBNCA>2.0.CO;2.

Rossi, G., Catani, F., Leoni, L., Segoni, S., Tofani, V., 2013. HIRESSS: a physically based slope stability simulator for HPC applications. Nat. Hazards Earth Syst. Sci. 13 (1), 151–166. https://doi.org/10.5194/nhess-13-151-2013.

Saco, P.M., Willgoose, G.R., Hancock, G.R., 2006. Spatial organization of soil depths using a landform evolution model. J. Geophys. Res.-Earth Surf. 111(2), F02016. doi:10.1029/2005JF000351.

Salciarini, D., Godt, J.W., Savage, W.Z., Conversini, P., Baum, R.L., Michael, J.A., 2006. Modeling regional initiation of rainfall-induced shallow landslides in the eastern Umbria Region of central Italy. Landslides 3, 181–194. https://doi.org/10.1007/s10346-006-0037-0.

Sameen, M.I., Pradhan, B., Lee, S., 2020. Application of convolutional neural networks featuring Bayesian optimization for landslide susceptibility assessment. Catena 186,. https://doi.org/10.1016/j.catena.2019.104249 104249.

Saulnier, G.M., Beven, K., Obled, C., 1997. Including spatially variable effective soil depths in TOPMODEL. J. Hydrol. 202, 158–172. https://doi.org/10.1016/S0022-1694(97)00059-0.

Segoni, S., Rossi, G., Catani, F., 2012. Improving basin scale shallow landslide modelling using reliable soil thickness maps. Nat. Hazards. 61 (1), 85–101. https://doi.org/10.1007/s11069-011-9770-3.

Segoni, S., Pappafico, G., Luti, T., Catani, F., 2020. Landslide susceptibility assessment in complex geological settings: Sensitivity to geological information and insights on its parameterization. Landslides 17, 1–11. https://doi.org/10.1007/s10346-019-01340-2.

Soldato, M.D., Segoni, S., Vita, P.D., Pazzi, V., Tofani, V., Moretti, S., 2016. Thickness model of pyroclastic soils along mountain slopes of Campania (southern Italy). In: Proc. 12th International Symposium on Landslides, Napoli, Italy, 797-804.

Soldato, M.D., Pazzi, V., Segoni, S., Vita, P.D., Tofani, V., Moretti, S., 2018. Spatial modeling of pyroclastic cover deposit thickness (depth to bedrock) in peri-volcanic areas of Campania (southern Italy). Earth Surf. Process. Landf. 43 (9), 1757–1767. https://doi.org/10.1002/esp.4350.

Tesfa, T.K., Tarboton, D.G., Chandler, D.G., McNamara, J.P., 2009. Modeling soil depth from topographic and land cover attributes. Water Resour. Res. 45 (10), W10438. https://doi.org/10.1029/2008WR007474.

Tofani, V., Bicocchi, G., Rossi, G., Segoni, S., D'Ambrosio, M., Casagli, N., Catani, F., 2017. Soil characterization for shallow landslides modeling: a case study in the Northern Apennines (Central Italy). Landslides 14 (2), 755–770. https://doi.org/10.1007/s10346-017-0809-8.

Tsai, C.C., Chen, Z.S., Duh, C.T., 2001. Prediction of soil depth using a soil-landscape regression model: a case study on forest soils in southern Taiwan. Proceedings of the National Science Council, Republic of China. Part B, Life sciences, 25(1), 34-39.

Tucker, G.E., Catani, F., Rinaldo, A., 2001. Statistical analysis of drainage density from digital terrain data. Geomorphology 36, 187–202. https://doi.org/10.1016/S0169-555X(00)00056-8.

Wang, H., Gao, J., Hou, W., 2019. Quantitative attribution analysis of soil erosion in different geomorphological types in karst areas: Based on the geodetector method. J. Geogr. Sci. 29 (2), 271–286. https://doi.org/10.1007/s11442-019-1596-z.

Wang, H.X., Liu, C.M., Yang, Z.F., 2001. Assessment and utilization of soil water resources. J. Geogr. Sci. 11 (1), 87–91. https://doi.org/10.1007/BF02837379.

Xiao, T., Yin, K.L., Yao, T.Y., Liu, S.H., 2019a. Spatial prediction of landslide susceptibility using GIS-based statistical and machine learning models in Wanzhou County, Three Gorges Reservoir, China. Acta Geochim. 38 (5), 1–16. https://doi.org/10.1007/s11631-019-00341-1.

Xiao, T., Segoni, S., Chen, L.X., Yin, K.L., Casagli, N., 2019b. A step beyond landslide susceptibility maps: a simple method to investigate and explain the different outcomes obtained by different approaches. Landslides 17, 627–640. https://doi.org/10.1007/s10346-019-01299-0.

Zhang, K.Q., Wang, L.Q., Dai, Z.W., Huang, B.L., Zhang, Z.H., 2022a. Evolution trend of the Huangyanwo rock mass under the action of reservoir water fluctuation. Nat. Hazards. 113, 1583–1600. https://doi.org/10.1007/s11069-022-05359-y.

Zhang, W.G., Li, H.R., Tang, L.B., Gu, X., Wang, L.Q., Wang, L., 2022b. Displacement prediction of Jiuxianping landslide using gated recurrent unit (GRU) networks. Acta Geotech 17, 1367–1382. https://doi.org/10.1007/s11440-022-01495-8.

Zhang, Y.H., Xu, X.L., Li, Z.W., Yi, R.Z., Xu, C.H., Luo, W., 2022c. Modelling soil thickness using environmental attributes in karst watersheds. Catena, 106053. https://doi.org/10.1016/j.catena.2022.106053.

Zhang, W.G., Wu, C.Z., Li, Y.Q., Wang, L., Samui, P., 2019. Assessment of pile drivability using random forest regression and multivariate adaptive regression splines. Georisk 10, 1–14. https://doi.org/10.1080/17499518.2019.1674340.

Zhang, W.G., Wu, C.Z., Zhong, H.Y., Li, Y.Q., Wang, L., 2021. Prediction of undrained shear strength using extreme gradient boosting and random forest based on Bayesian optimization. Geosci. Front. 12 (1), 469–477. https://doi.org/10.1016/j.gsf.2020.03.007.

Zhou, X.Z., Wen, H.J., Zhang, Y.L., Xu, J.H., Zhang, W.G., 2021. Landslide susceptibility mapping using hybrid random forest with GeoDetector and RFE for factor optimization. Geosci. Front. 12, (5). https://doi.org/10.1016/j.gsf.2021.101211 101211.